

Reduction of Middle-Atmospheric Forecast Bias through Improvement in Satellite Radiance Quality Control

YOUNG-JOON KIM, WILLIAM F. CAMPBELL, AND STEVEN D. SWADLEY

Naval Research Laboratory, Monterey, California

(Manuscript received 13 July 2009, in final form 27 October 2009)

ABSTRACT

This article discusses a practical problem faced in operational atmospheric forecasting and data assimilation, and efforts to improve forecast quality through the choice of quality control parameters. The need to utilize as much data as possible must be carefully balanced against the need to reject observations deemed erroneous because they are far from the background value. Alleviation of forecast bias in the middle atmosphere for a global atmospheric prediction system is attempted via improvement of the quality control and bias correction of the satellite radiance data; in particular, the sensitivity of the analysis to the satellite radiance outlier check parameters for the Naval Research Laboratory's three-dimensional variational data assimilation system [Naval Research Laboratory Atmospheric Variational Data Assimilation System (NAVDAS)] is investigated. A series of forecast experiments are performed with an extended-top (0.04 hPa or ~65 km) version of the U.S. Navy's Operational Global Atmospheric Prediction System (NOGAPS) for the month of January 2007. The experiments vary the prescribed radiance observation error variance for the Advanced Microwave Sounding Unit-A (AMSU-A) and the tolerance factors for the AMSU-A and NAVDAS quality control processes. The biases of geopotential height, temperature, and wind in the middle atmosphere are significantly reduced when the observation error limit for the highest-altitude AMSU-A channel (i.e., 14) is relaxed from 0.95 to 3 K and the tolerance factors for the AMSU-A and NAVDAS quality control processes are relaxed from 3 to 4. The improvement is due to assimilation of more high quality AMSU-A radiance data from the highest-peaking channel.

1. Introduction

The goal of atmospheric data assimilation is to determine the best estimate (*analysis*) of the current state of the atmosphere, given a prior estimate of the current state (*background*, typically a 6-h forecast from a numerical model), and current observations of the atmosphere. This study is concerned solely with microwave satellite radiances, which can be used to infer the temperature structure of the atmosphere (in concert with other conventional and satellite radiances). Polar-orbiting satellite observations are somewhat irregular in time and space, are sparse compared to the numerical model state, and have both systematic errors (biases) and random errors. The forecast models that provide the background information are dynamically consistent, but they also have biases, particularly in the stratosphere. The

challenge of data assimilation is to transfer information from the scattered locations and times of the observations to the model grid, while preserving the physical, dynamical, and numerical consistency that is essential to making consistently good weather forecasts.

This study addresses a practical problem faced in the assimilation of radiance data obtained from the Advanced Microwave Sounding Unit-A (AMSU-A, a cross-track microwave radiometer for temperature sounding) instruments aboard National Oceanic and Atmospheric Administration (NOAA) satellites in the Naval Research Laboratory's Atmospheric Variational Data Assimilation System (NAVDAS; Daley and Barker 2001a,b), the operational three-dimensional variational data assimilation system at the Fleet Numerical Meteorology and Oceanography Center (FNMOC).¹ There are two parts

Corresponding author address: Dr. Young-Joon Kim, Marine Meteorology Division, Naval Research Laboratory, Stop 2, Monterey, CA 93943.
E-mail: yj.kim@nrlmry.navy.mil

¹ On 23 September 2009, after the manuscript was written, the NAVDAS was replaced at FNMOC by NAVDAS-AR, a global 4DVAR system based on accelerated representer algorithms, together with an upgraded version of the NOGAPS forecast model extending to 0.04 hPa.

Report Documentation Page

Form Approved
OMB No. 0704-0188

Public reporting burden for the collection of information is estimated to average 1 hour per response, including the time for reviewing instructions, searching existing data sources, gathering and maintaining the data needed, and completing and reviewing the collection of information. Send comments regarding this burden estimate or any other aspect of this collection of information, including suggestions for reducing this burden, to Washington Headquarters Services, Directorate for Information Operations and Reports, 1215 Jefferson Davis Highway, Suite 1204, Arlington VA 22202-4302. Respondents should be aware that notwithstanding any other provision of law, no person shall be subject to a penalty for failing to comply with a collection of information if it does not display a currently valid OMB control number.

1. REPORT DATE 27 OCT 2009	2. REPORT TYPE	3. DATES COVERED 00-00-2009 to 00-00-2009			
4. TITLE AND SUBTITLE Reduction of Middle-Atmospheric Forecast Bias through Improvement in Satellite Radiance Quality Control		5a. CONTRACT NUMBER			
		5b. GRANT NUMBER			
		5c. PROGRAM ELEMENT NUMBER			
6. AUTHOR(S)		5d. PROJECT NUMBER			
		5e. TASK NUMBER			
		5f. WORK UNIT NUMBER			
7. PERFORMING ORGANIZATION NAME(S) AND ADDRESS(ES) Naval Research Laboratory, 7 Grace Hopper Ave, Monterey, CA, 93943		8. PERFORMING ORGANIZATION REPORT NUMBER			
9. SPONSORING/MONITORING AGENCY NAME(S) AND ADDRESS(ES)		10. SPONSOR/MONITOR'S ACRONYM(S)			
		11. SPONSOR/MONITOR'S REPORT NUMBER(S)			
12. DISTRIBUTION/AVAILABILITY STATEMENT Approved for public release; distribution unlimited					
13. SUPPLEMENTARY NOTES					
14. ABSTRACT					
15. SUBJECT TERMS					
16. SECURITY CLASSIFICATION OF:			17. LIMITATION OF ABSTRACT Same as Report (SAR)	18. NUMBER OF PAGES 20	19a. NAME OF RESPONSIBLE PERSON
a. REPORT unclassified	b. ABSTRACT unclassified	c. THIS PAGE unclassified			

to NAVDAS: the data preparation algorithms that form the differences between the observations and the background (*innovations*), and the solver that turns innovations into corrections, which are added to the background to form the analysis. Throughout this study, references to NAVDAS may indicate either the entire NAVDAS system, or simply the solver that takes innovations and produces corrections; context will make it clear which is the correct meaning.

Data assimilation procedures typically begin with quality control (QC) procedures to mitigate errors in the observation data. Our QC procedures for AMSU-A radiances include elimination of redundant data, screening of known bad satellite channels and low-peaking channels over land–sea ice, gross error checks for unphysical values, an innovation outlier check (controlled by the AMSU-A tolerance factor) to eliminate data that are statistically unlikely given the forecast, and a buddy check (controlled by the NAVDAS tolerance factor) to eliminate data that are statistically unlikely given the neighboring observations (Baker and Campbell 2004; Baker et al. 2005). Details of the QC procedures are given in appendix A.

Data assimilation systems require an accurate, unbiased background, in our case a 6-h model forecast. If the model atmosphere is biased, valuable observations can be rejected by the QC procedures when the innovation magnitude exceeds a prescribed limit. For example, if the model background is systematically too cold with respect to the observations, good observations warmer than the background (warm tail) will be discarded, while bad observations colder than the background (cold tail) will be retained, because the global distribution of innovations is assumed to be approximately Gaussian and centered on zero. Thus, the observations will not do as good a job of warming the model, and some very bad cold observations will have a disproportionate negative effect. In addition, the bias correction of satellite radiances, which is performed after the initial QC but before the innovation outlier check and buddy check, can be adversely affected by the initial QC, and can adversely affect the results of subsequent QC. If the innovation limit is relaxed excessively, however, significant errors can be introduced and the forecast skill can be degraded. Innovation limits must be set properly, which is difficult to do objectively because currently most data assimilation systems are bias blind, designed only to correct random error rather than systematic error. Development of true bias-aware bias correction algorithms is an active research topic (see, e.g., Dee 2005).

In addition to imperfect observations and imperfect forecasts, data assimilation systems require a third source of information: the observation and background error

covariance matrices. These error covariances determine the relative weights given to the forecast and the observations, and are used to spread information from observed quantities and observation locations throughout the entire space of the model. For this study, we used the background error covariances specified in NAVDAS. For some experiments the observation error variances for AMSU-A radiances were modified, which affects the relative weights of the background and observations in determining the analysis. Interested readers are referred to appendix B for a brief description of variational data assimilation or to Daley and Barker (2001a,b) for more details.

For stratospheric data assimilation, a major source of bias is model error, and observation bias (Dee 2005) is a complicating factor. To improve middle-atmospheric forecasts with an extended-top version of the Navy Operational Global Atmospheric Prediction System (NOGAPS; Hogan and Rosmond 1991), Kim (2007) introduced improved middle-atmospheric physics with an additional gravity wave drag parameterization, which has a great impact on the middle atmosphere. The present study addresses the other component of the forecast system (i.e., the data assimilation system); in particular, the interaction of QC and bias correction of microwave radiances in NAVDAS in the middle atmosphere.

The sensitivity of the analysis to the satellite radiance innovation outlier check in the middle atmosphere is investigated using AMSU-A radiance data. A series of forecast experiments are performed varying three parameters: the observation error variance prescribed in operational NAVDAS, and the tolerance factors for both the AMSU-A innovation outlier check and the NAVDAS buddy check. The observation error variance includes satellite instrument error, error in the radiative transfer model, and error of representativeness. It helps to determine how closely NAVDAS will draw to an observation relative to the background: the larger it is, the less influence the observations have on the analysis. The innovation limit is defined as a tolerance factor multiplied by the observation error standard deviation, and is the threshold for the innovation outlier check in the AMSU-A data preparation algorithm (appendix A) and the buddy check in the NAVDAS solver. In some experiments, relaxed innovation limits are applied to all AMSU-A channels; in others, they are applied only to the highest-peaking middle-atmospheric channel (channel 14; Fig. 1). Our hypothesis is that the relaxed limits will allow more good radiance data to pass the innovation outlier check and be available to correct the model bias, because the default limits allow only a small percentage of available data from channel 14 to be assimilated.

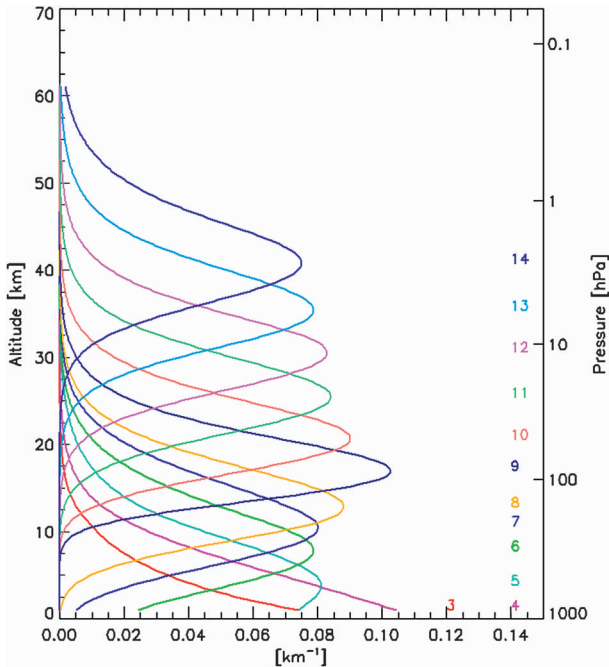


FIG. 1. Weighting functions at nadir for the AMSU-A instrument on the NOAA satellites for the *U.S. Standard Atmosphere, 1976*. The highest peaking channel (14) is sensitive to temperatures at altitudes as high as about 60 km and as low as about 25 km, with peak sensitivity near 40 km.

Our results show that the forecast bias in the middle atmosphere can be mitigated when the parameters are selected in certain combinations that allow more data to pass the innovation outlier check, but selectively for high altitudes. [Note that Auligné and McNally (2007) explored the interaction between bias correction and QC, and discussed the influence of residual outliers and an asymmetric QC. The present study investigates the impacts of changes in the data outlier check for the NOGAPS/NAVDAS QC procedures on the bias correction in terms of actual forecast bias in the stratosphere.] Section 2 describes the details of the experiments. The results are presented and discussed in section 3. Further remarks are given in section 4. Appendix A describes the details of the bias correction–quality control procedure and appendix B provides a concise description of the analysis equations used for the NOGAPS/NAVDAS system.

2. Experimental setup

A version of the NOGAPS/NAVDAS system with its top raised from 4 hPa (~40 km) to 0.04 hPa (~65 km) is used for this study. The horizontal and vertical resolutions of the forecast model are T239 (triangular spectral truncation at wavenumber 239, or ~0.5° in latitude)

and L42 (42 levels), respectively. A similar extended-top research version of NOGAPS was used earlier by Kim and Hogan (2004), but the version used here includes the FNMOC operational physics package, which does not include adequate middle-atmospheric physics. The radiance bias correction (appendix A) method follows the operational one (Baker and Campbell 2004; Baker et al. 2005), which is based on Harris and Kelly (2001) except that only two predictors (850–300- and 200–50-hPa geopotential height thicknesses) were used. Surface skin temperature and total-column water vapor were not used because channel 14 is insensitive to both water and the surface (see appendix B for more information). The full FNMOC operational dataset was used. It did not include any stratospheric observations other than radiosondes and AMSU-A radiances. The coefficients for the radiance bias correction were obtained from a previous research run for 0000 UTC 5 December–20 December 2006. The coefficients were not updated in time during the forecast experiment in order to eliminate the potential feedback effect that can occur between QC and bias correction (Auligné and McNally 2007). (Note that the Met Office successfully uses nonadaptive bias correction, manually updating the coefficients every few months.) For each experiment, cycling data assimilation was run from 0000 UTC 20 December 2006 to 1800 UTC 31 January 2007. Five-day forecasts were launched once a day from the 0000 UTC analysis, starting at 0000 UTC 27 December 2006.

The sensitivity experiments include one or more of the following modifications:

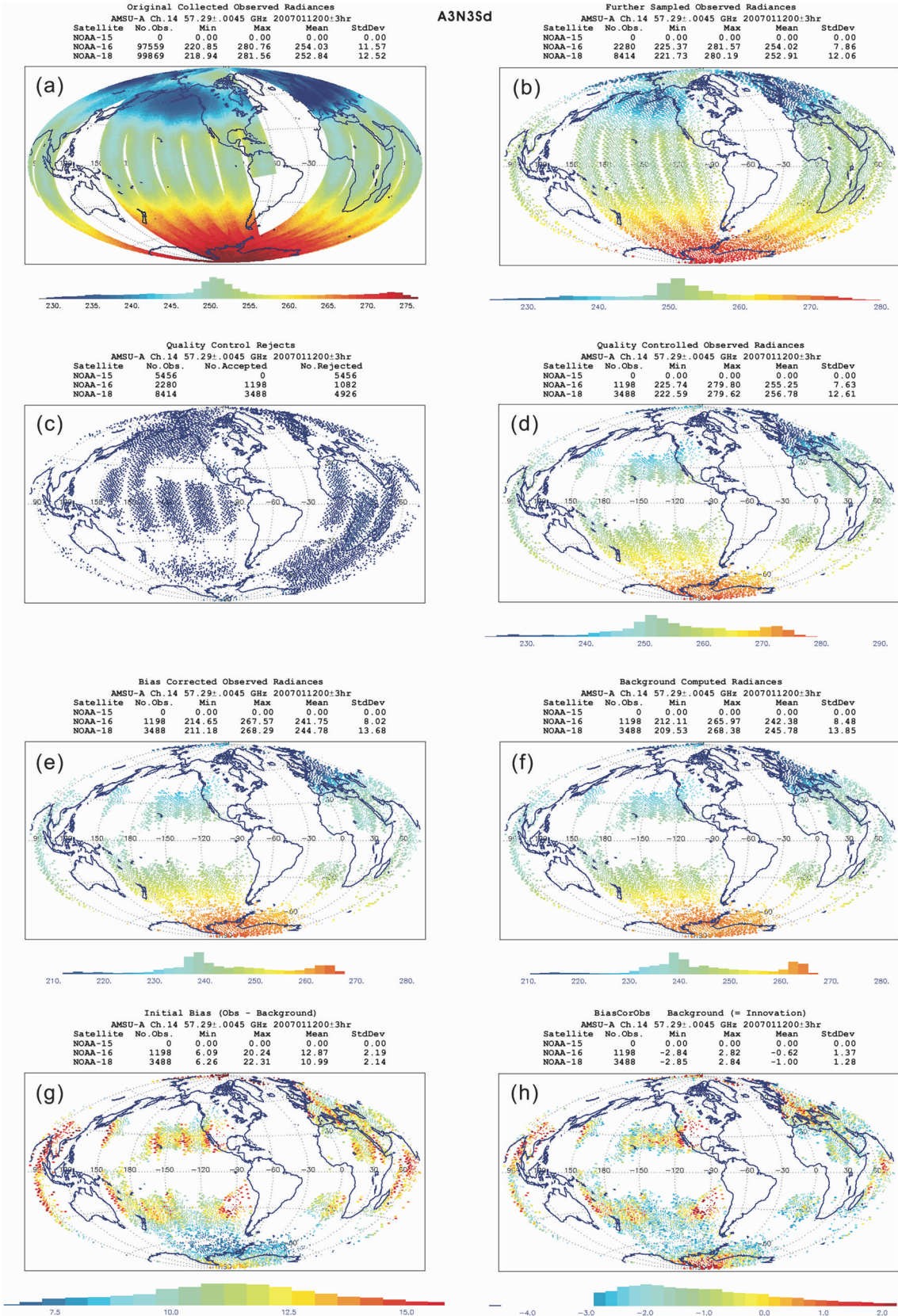
- 1) an increase in the AMSU-A QC tolerance factor from 3 (default value) to 4, denoted respectively as A3 and A4;
- 2) an increase in the NAVDAS tolerance factor from 3 (default value) to 4, denoted respectively as N3 and N4;
- 3) an increase in the observation standard deviation (σ) for AMSU-A channel 14 from 0.95 K (default value) to 3.0 K, denoted respectively as Sd and S3; and
- 4) an increase in the AMSU-A QC tolerance factor to 4 for the highest-altitude AMSU-A channel (i.e., ch14) only, denoted as A4(14).

The default set of parameters, currently adopted for operational NOGAPS, can be thus denoted as A3N3Sd and the set with maximum relaxation as A4N4S3.

3. Results and discussions

a. Control run

Figure 2 shows an example of the global distribution of the satellite radiance data obtained from each step of the bias correction procedures for AMSU-A channel 14



in the NOGAPS/NAVDAS system (see appendix A for details) for the control run, with the default values of the observation error variance and the default tolerance factors. Channel 14 is the highest-peaking channel covering the highest altitudes near the model top of 0.04 hPa or ~ 65 km (see Fig. 1). The observed radiance data are collected for the 6-h windows centered on 0000 UTC 12 January 2007. The collected data (Fig. 2a) are further sampled (Fig. 2b) to remove redundant data. As noted earlier, the default error tolerance factors for the AMSU-A and NAVDAS routines and the default observation error variances are 3, 3, and 0.95 K, respectively. The locations of the rejected data are shown in Fig. 2c. After various QC procedures, including the innovation outlier check controlled by the innovation limit for AMSU-A, the accepted data are shown in Fig. 2d.

As summarized in Table 1 (see case A3N3Sd), the data usage rate is overall quite low (note the usage rate comes after step 2 in appendix A and corresponds to Fig. 2d). The data from *NOAA-15* are rejected entirely due to the failure of channel 14. The total usage rates of the sampled data for *NOAA-16* and *-18* after the initial QC are 52.5% and 41.5%, respectively. Figure 2f presents the background radiances calculated from the forecast model, which are collocated with the quality controlled, bias-corrected observations (Fig. 2e). Figures 2g and 2h show the difference between the observation and the model background, before (Fig. 2g) and after (Fig. 2h) the bias correction. The latter (Fig. 2h) is also referred to as the *innovation*, which is the key information needed for the data assimilation. The most strikingly problematic feature is the large amount of good observation data that has been rejected by the QC process (Fig. 2c).

Figure 2 also includes the corresponding histograms. The sampled radiance data are centered and peaked around 251 K with rough symmetry with respect to the mean (Fig. 2b), but become rather asymmetric after the QC process (Fig. 2d) with an increased amount of higher-temperature data centered around 273 K. The bias correction process shifts the distribution to lower temperature (to around 239 K) by about 12 K while approximately maintaining its original shape (Fig. 2e). The innovation (Fig. 2h) is quite different from the initial

difference (Fig. 2g). The initial bias (Fig. 2g) is approximately in normal distribution with respect to the mean value of 11 K (meaning the observations are systematically warmer than the background). The innovation (Fig. 2h) is severely skewed to the negative side, implying colder observation data, although their magnitudes are much smaller than that of the initial bias (Fig. 2g). The peak of the distribution is centered on -2 K (Fig. 2h), which shows that the mean innovation on this day differed by 2 K from the mean innovation of the 15-day training set used to create the radiance bias correction coefficients. Due to the 2-K bias, the 3σ innovation limit cuts off a relatively large portion of the negative (left) flank of the data, which could have been useful for bias correction, simultaneously violating the assumption of normally distributed observation errors (appendix B). One possible strategy to mitigate this effect is to compute standardized regression coefficients on the training set for radiance bias correction, and subtract the mean innovation of the day before applying the coefficients; however, our software considers innovations serially, which made it difficult to use that strategy in this study. (Because there is QC that happens *after* the bias correction step, it may be that the innovations that went into the regression have a systematic difference from the innovations at the bias correction stage, which is another possible explanation for the 2-K difference, but we think this is unlikely.)

Figure 3a displays a scatterplot of the quality controlled innovations (Fig. 2g) versus the bias-corrected innovations (Fig. 2h) for channel 14 of *NOAA-18*'s radiances, color coded by latitude. The 3σ innovation check excludes data outside of the box ($\pm 3 \times 0.95$ K). The quality controlled innovations are largely skewed toward the positive (due to cold model background) whereas the bias-corrected innovations are well centered with respect to zero. The latitudinal distribution reveals that most of the data in the northern polar areas (represented by red crosses) are thrown out, as is a significant amount of data in the tropics (greenish crosses).

Next, we verify selected forecast fields against analysis fields obtained from the control run of the extended-top system. We compare the 3-day forecast started from

←

FIG. 2. Global distribution of the *NOAA-15*, *-16*, and *-18* satellite radiance data obtained from each step of the bias correction procedure for AMSU-A channel 14 with the default set of parameters (A3N3Sd) in the NOGAPS/NAVDAS system. The data are collected from the control experiment for the 6-h windows centered on 0000 UTC 12 Jan 2007. (a) Original collected observed; (b) further sampled observed; (c) observed rejected by QC; (d) quality controlled observed; (e) quality controlled and bias-corrected observed; (f) model-background computed; (g) initial quality controlled and scan corrected, observed minus background; and (h) bias-corrected observed minus background (i.e., innovation) radiances. Note that (h) is not a bell curve because the left tail was cut off by the uncentered innovation limit.

TABLE 1. The number of satellite radiance observations (after step 2 in appendix A) for the AMSU-A channel 14 centered at 0000 (± 3 h) UTC 12 Jan 2007 and the corresponding usage rates for each satellite and experiment (experiment A3N3Sd corresponds to Fig. 2d). The data from *NOAA-15* were excluded due to the failure of channel 14, which demonstrates that a satellite instrument can fail anytime, uncontrollably degrading data assimilation with satellite data.

Expt	Satellite	No. of radiance observations	Usage rate (%)
Pre-QC	<i>NOAA-15</i>	5456	0
	<i>NOAA-16</i>	2280	0
	<i>NOAA-18</i>	8414	0
	Sum	16 150	0
A3N3Sd	<i>NOAA-15</i>	0	0
	<i>NOAA-16</i>	1198	52.5
	<i>NOAA-18</i>	3488	41.5
	Sum	4686	29.0
A3N3S3	<i>NOAA-15</i>	0	0
	<i>NOAA-16</i>	1374	60.3
	<i>NOAA-18</i>	4329	51.5
	Sum	5703	35.3
A4N3Sd	<i>NOAA-15</i>	0	0
	<i>NOAA-16</i>	1393	61.1
	<i>NOAA-18</i>	4332	51.5
	Sum	5725	35.5
A4N3S3	<i>NOAA-15</i>	0	0
	<i>NOAA-16</i>	1405	61.6
	<i>NOAA-18</i>	4277	50.8
	Sum	5682	35.2

0000 UTC 12 January 2007 with the analysis at 0000 UTC 15 January 2007. Comparison of the analyzed (Fig. 4a) and forecast (Fig. 4b) zonal-mean zonal wind reveals significant bias in the high latitudes in the upper stratosphere and over the South Pole in the lower stratosphere (Fig. 4c), although they compare relatively well overall. The corresponding temperatures (Fig. 5) reveal a level of bias that is somewhat similar to the wind counterpart, notably the cold model bias in the northern polar upper stratosphere (Fig. 5c). Unlike the wind bias, however, the significant (warm) bias around 10 hPa is widespread. The large positive zonal wind bias, found in the northern stratosphere over high latitudes (Fig. 4c), is associated with the large cold bias in the upper stratosphere near the North Pole (Fig. 5c) through the thermal wind relation. This bias cannot be alleviated systematically by data assimilation because a large amount of the

observation data in the northern polar region has been rejected by the QC process (Figs. 2c and 3) and is thus not available to influence the analysis.

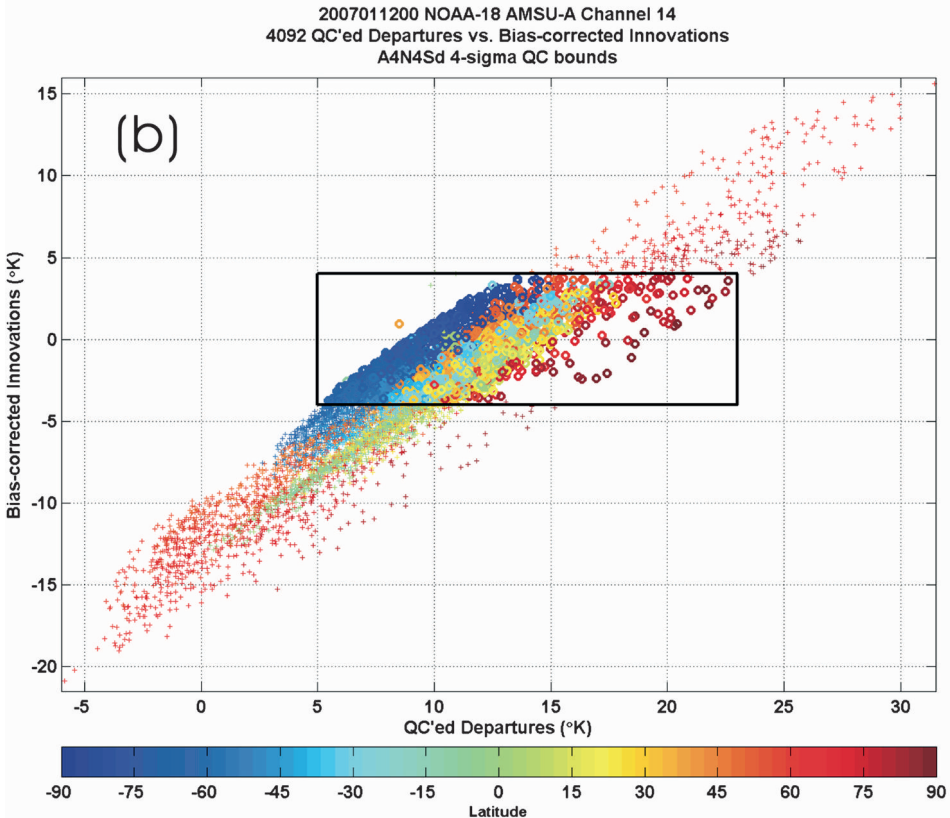
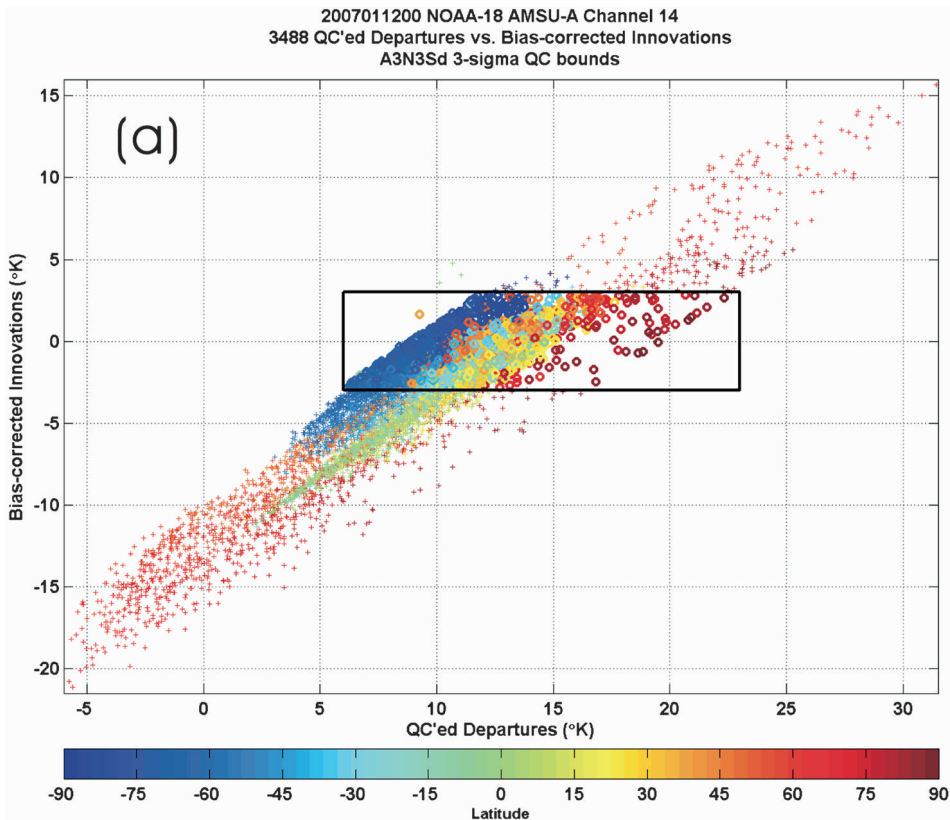
The skill of the stratospheric forecast for January 2007 is given in Fig. 6 in terms of the root-mean-square (RMS) error for the geopotential height (Fig. 6a), temperature (Fig. 6b), and vector wind (Fig. 6c). The skill scores were calculated with respect to self-analysis, as is conventionally done in global data assimilation. Higher skill (lower RMS error) means that the forecast agrees better with the analysis, but not necessarily with the real atmosphere. The errors grew in time, as expected, and the skill was worse at higher altitudes, consistent with the larger errors shown in Figs. 4 and 5. The largest errors for the height and wind were found in the Northern Hemisphere at 1 hPa, while those for the temperature were in the tropics, also at 1 hPa (see the temperature error in Fig. 5c).

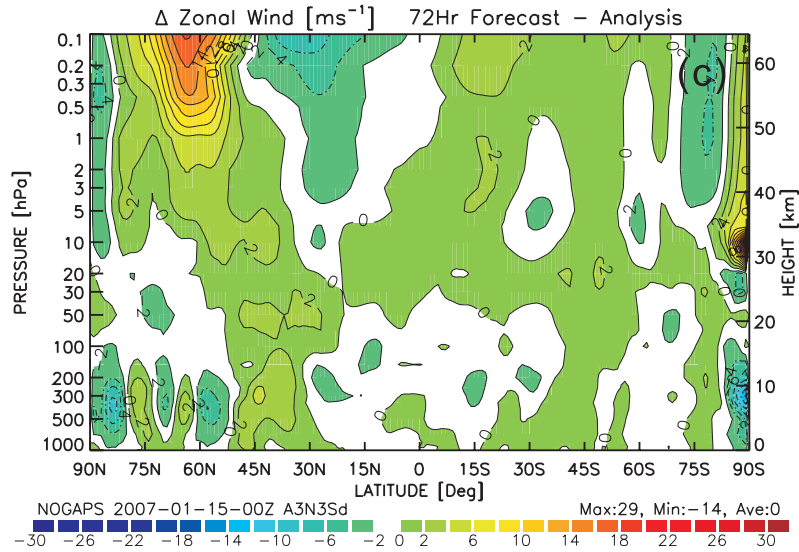
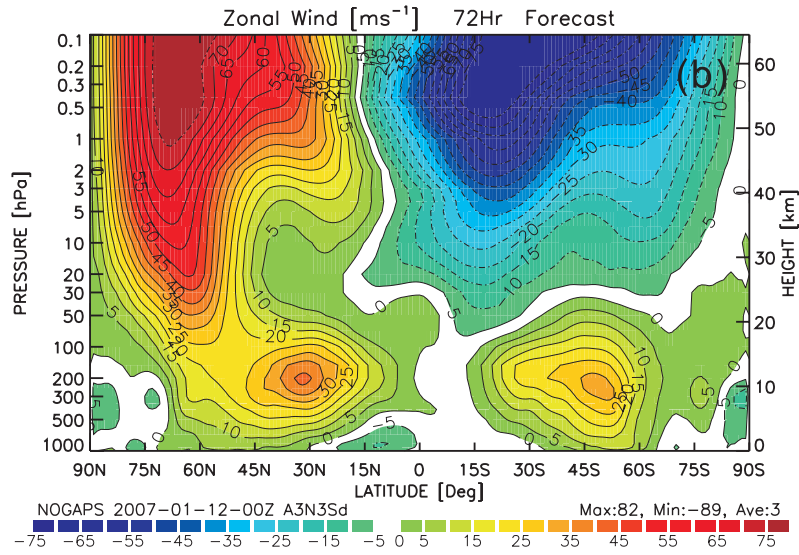
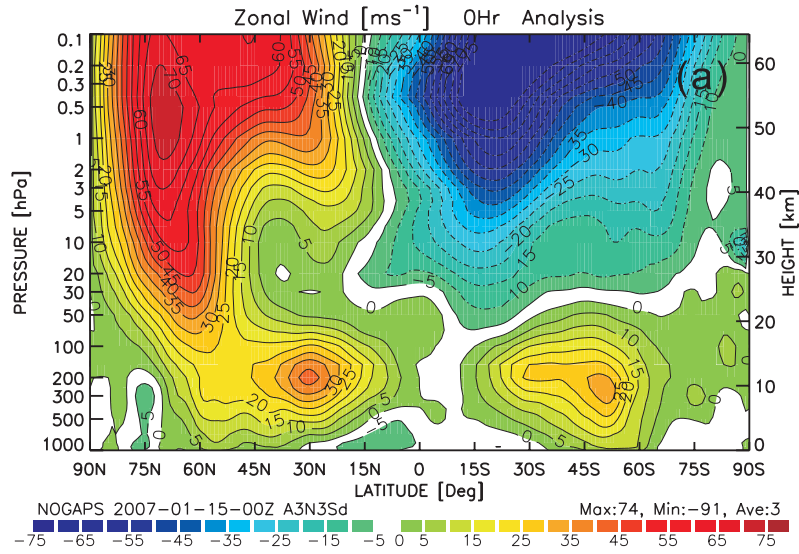
b. Experimental runs with relaxed innovation limits

We investigate here whether forecast skill can be improved by adjusting the QC process in order to make more data, presumably of good quality, available for assimilation. The innovation limits were relaxed based on the assumption that the default set of parameters undesirably rejects potentially useful data during the QC process. Experiments with the combinations of the error tolerance factors for AMSU-A and NAVDAS, which are changed from 3 to 4, and the observation error changed from the default value of 0.95 K to 3.00 (see Table 2) were performed. Changing the assumed observation error variance itself had a larger impact than changing the tolerance factors in expanding the allowed innovation range (see Fig. 7). Moreover, because the AMSU-A quality control is performed first and its final product, the innovation, is fed into the NAVDAS process, the impacts of the NAVDAS tolerance factor are usually smaller than those of AMSU-A tolerance factor.

Figure 8 compares the number of satellite radiance observations and data usage rates for the 6-h window centered on 0000 UTC 12 January 2007 (see Fig. 2) from all experiments. The number of observations increases when the innovation limits are relaxed. In particular, the forecast with all parameters relaxed (A4N4S3) increased the number of observations almost by 50% in

FIG. 3. A scatterplot of the quality controlled (i.e., initial) departures (Fig. 2g) vs the bias-corrected innovations (Fig. 2h) for channel 14 of *NOAA-18* radiances, color coded with respect to the latitude, with the (a) default (A3N3Sd, i.e., $\sigma = 0.95$; $-3\sigma \sim 3\sigma$, corresponding to Fig. 2) and (b) maximum-relaxed (A4N4S3, i.e., $\sigma = 3.00$; $-4\sigma \sim 4\sigma$) ranges of the innovation limit. The rectangular box represents the radiance data available for the bias correction. The left and right sides of the box are drawn to represent the end of the data points.





comparison with the default case (A3N3Sd). Figure 9 shows the rejections (left panel) and the quality controlled radiances (right panel). In comparison with the control case, A3N3Sd (Figs. 2c and 2d, respectively), much less of the data is rejected for the relaxed case (A4N4S3; bottom panel) especially over the southern Atlantic Ocean (west of Chile), Southern Africa, the subtropical Pacific, and the Southern Ocean. We compare the scatterplots of the control case (Fig. 3a) and this relaxed case (A4N4S3; Fig. 3b). The relaxed case clearly includes more data in all latitudes.

The changes of A3 to A4 and Sd to S3 both increase the number of observations by 22% (Table 1). A greater number of observations available for the bias correction, however, does not necessarily guarantee improved forecasts in the middle atmosphere. Figures 10 and 11 compare among the cases the RMS errors of the geopotential height, horizontal wind, and temperature of the 3-day forecasts at 1 hPa (Fig. 10) and at 10 hPa (Fig. 11) for January 2007. The errors for A4N4S3, which include the greatest number of observations, are consistently worse than the control (A3N3Sd). The errors from A3N3Sd and A3N3S3 are, overall, smaller than those from other cases (except for those cases that relax channel 14 only, which will be described later).

Increasing the amount of observational data can introduce radiance data of poor quality, which likely explains the degradations noted above. The forecast model is known to be significantly biased in the upper stratosphere, so we subsequently restricted the innovation limit changes to channel 14, whose weighting function peaks around 40 km and is sensitive between 30 and 55 km (see Fig. 1), and repeated the forecast experiments. The results reveal significantly reduced RMS errors for January 2007 (Figs. 10 and 11) regardless of the tolerance factor for NAVDAS or the observation error variance [see any A4(14) cases], with a notable exception of the temperature bias at 1 hPa in the tropics (Fig. 10c). Use of more high-altitude data improved the quality of the innovation vector and reduced the bias. This suggests that the default set of the tolerance factors and the observation error, which were calibrated for the operational version of NOGAPS/NAVDAS with its top at 1 hPa, are generally effective only at pressures greater than 1 hPa (lower in height). The same set of parameters is not optimal (probably too small) for the higher levels between 1 and 0.1 hPa or above 50 km.

Figures 12 and 13 show the time series of the RMS height errors at 1 hPa (Fig. 12) and 10 hPa (Fig. 13) from the 3-day forecasts for the entire month of January 2007. Figures 12 and 13 show an initial spinup period for all experiments. While the errors for the different experiments in the Northern Hemisphere do not differ significantly from one another, the errors in the Southern Hemisphere are dramatically reduced in the stratosphere for the experiments in which only channel 14 is relaxed (denoted by brown and black dashed-dotted lines). Figures 12 and 13 clearly demonstrate that the selective, additional upper-stratospheric data, which became available with the relaxed limits, are beneficial. The additional data alleviated the model error in the stratosphere and, thus, improved the forecasts of the middle atmosphere in the Southern Hemisphere.

Figures 14 (zonal wind bias) and 15 (temperature bias) confirm that relaxing the AMSU-A tolerance factor only for channel 14 (Figs. 14c and 15c; cf. with Figs. 4c and 5c, respectively) is more effective in reducing the model bias. In particular, the wind bias in Fig. 14c resembles the typical bias found in large-scale models, and the temperature bias in Fig. 15c is significantly smaller than other cases especially around 10 hPa throughout the latitudes. Table 3 summarizes the bias for the zonal wind and temperature fields in terms of the maximum value of the bias fields (forecast minus analysis), the minimum value of the bias fields, and the difference between the two, for the zonal mean zonal wind (three columns in the left from left), and similarly for the zonal temperature (three columns in the right). Note that the A4(14) experiments show considerably smaller zonal wind $[(U_F - U_A)_{\max} - (U_F - U_A)_{\min}]$ and temperature $[(T_F - T_A)_{\max} - (T_F - T_A)_{\min}]$ errors than does the control. Table 3 confirms that the largest reductions of the extreme wind and temperature errors are found in cases with the AMSU-A error tolerance factor relaxed for channel 14 only, consistent with Figs. 10 and 11.

4. Further remarks

From a data assimilation perspective, atmospheric forecast skill should respond positively to an increase in the quantity and/or quality of the observational data; however, careful quality control (QC) is needed to see a benefit from an increased quantity of satellite radiance data. The present study demonstrates that more radiance

←

FIG. 4. The (a) analysis, (b) forecast, and (c) forecast minus analysis of the zonal-mean zonal wind, obtained from the NOGAPS control run (A3N3Sd). The 3-day forecast started from 0000 UTC 12 Jan 2007 is verified by the analysis at 0000 UTC 15 Jan 2007.

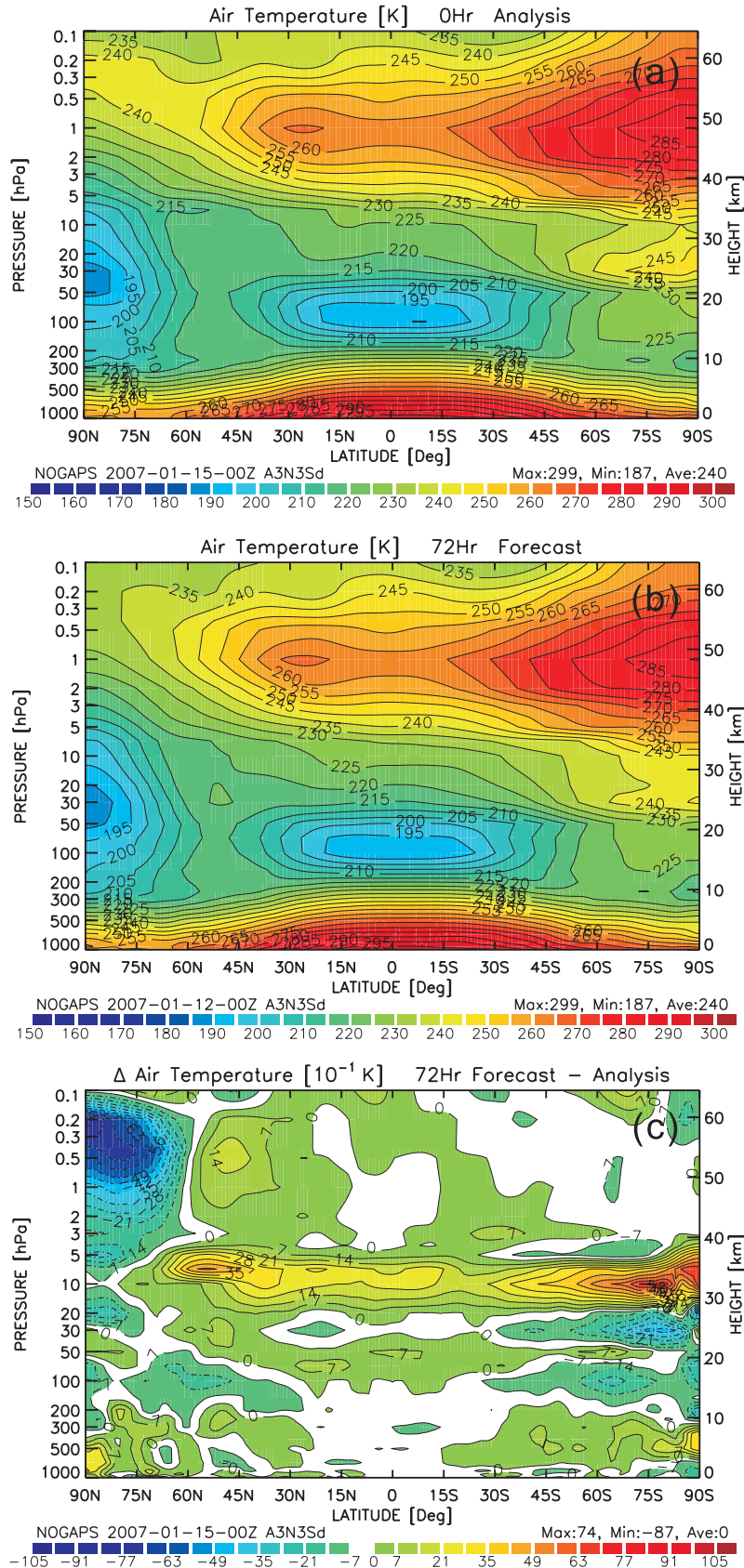


FIG. 5. As in Fig. 4, but for the temperature.

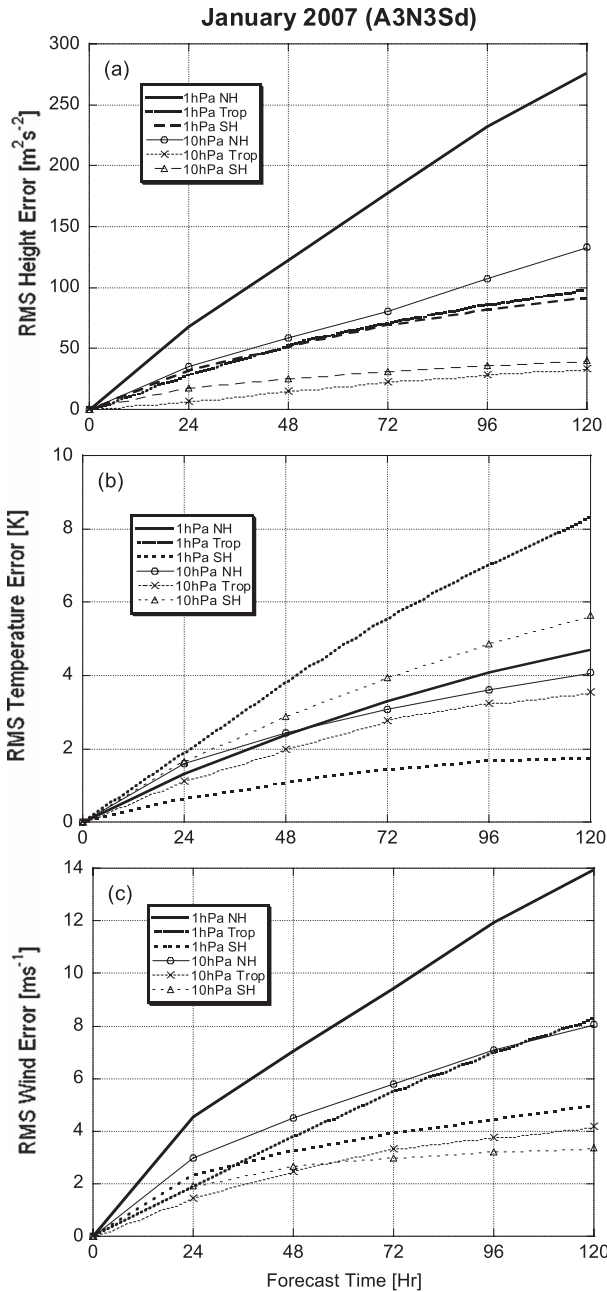


FIG. 6. The RMS errors of the NOGAPS control (A3N3Sd) forecasts averaged for January 2007 for the (a) geopotential height ($m^2 s^{-2}$), (b) temperature (K), and (c) vector wind ($m s^{-1}$) at 1 and 10 hPa in the Northern Hemisphere (NH; $20^\circ \sim 80^\circ N$), Southern Hemisphere (SH; $20^\circ \sim 80^\circ S$), and tropics (Trop; $20^\circ S \sim 20^\circ N$).

data can be beneficial with the selected middle-atmospheric channel (channel 14) of the AMSU-A instrument. The simple methodology used in this study can be applied to any similar bias-blind bias correction algorithms that use fixed-observation errors and tolerance factors. It can also be applied to radiance data from any source [e.g.,

TABLE 2. The innovation limit values for each experiment, with respect to the given observation error ($\sigma = 0.95$ or 3.00) and tolerance factors (3 or 4) for the AMSU-A and NAVDAS quality control procedures. The innovation limit is defined as the tolerance factor times the observation error. See Fig. 7 for a graphical comparison.

Expt	σ	Innovation limit for AMSU-A	Innovation limit for NAVDAS
A3N3Sd	0.95	$3\sigma = 2.85$	$3\sigma = 2.85$
A3N3S3	3.00	$3\sigma = 9.00$	$3\sigma = 9.00$
A3N4Sd	0.95	$3\sigma = 2.85$	$4\sigma = 3.80$
A3N4S3	3.00	$3\sigma = 9.00$	$4\sigma = 12.00$
A4N3Sd	0.95	$4\sigma = 3.80$	$3\sigma = 2.85$
A4N3S3	3.00	$4\sigma = 12.00$	$3\sigma = 9.00$
A4N4Sd	0.95	$4\sigma = 3.80$	$4\sigma = 3.80$
A4N4S3	3.00	$4\sigma = 12.00$	$4\sigma = 12.00$

the Special Sensor Microwave Imager Sounder (SSMIS), which covers altitudes approaching 80 km).

There are a number of factors chosen in this study that can be further improved. First, the modified Harris–Kelly bias correction does not include a predictor in the middle atmosphere. One could add, for example, a 30–10-hPa-thickness predictor, which was considered in an early draft of the Harris–Kelly paper. As was mentioned in section 3a, applying innovation limits centered on the mean innovation of the day, rather than zero, should improve the analysis in the upper stratosphere. Adaptive bias coefficient updating could be used as well, as it is in the operational data assimilation at FNMOC. Our study focused on the impacts of channel 14, the highest-peaking AMSU-A channel (Fig. 1), but other channels (e.g., 13) also cover high altitudes and may need to be included in future studies. Variational bias correction systems are used in some operational centers to automate the bias correction procedure, but they are *not* typically used on stratospheric channels such as AMSU-A channel 14 (Dee and Uppala 2008). The radiative transfer algorithm we used did not incorporate the Zeeman splitting effect for the highest-peaking microwave channel, although its effect is less than 1 K for channel 14 and negligible for lower-peaking channels.

Furthermore, we investigated only one month in boreal winter. It would be of interest to repeat the experiments for other seasons, and for sudden stratospheric warming events. This study focused on the middle atmosphere in terms of RMS errors. Our results are mixed at lower levels, depending on geographic regions and altitudes. We are currently investigating a means of systematically limiting the parameter modifications to a selected geographical area (e.g., the Southern Hemisphere, where we obtained the most improvement) to retain the upper-level improvement while leaving the lower levels unaffected.

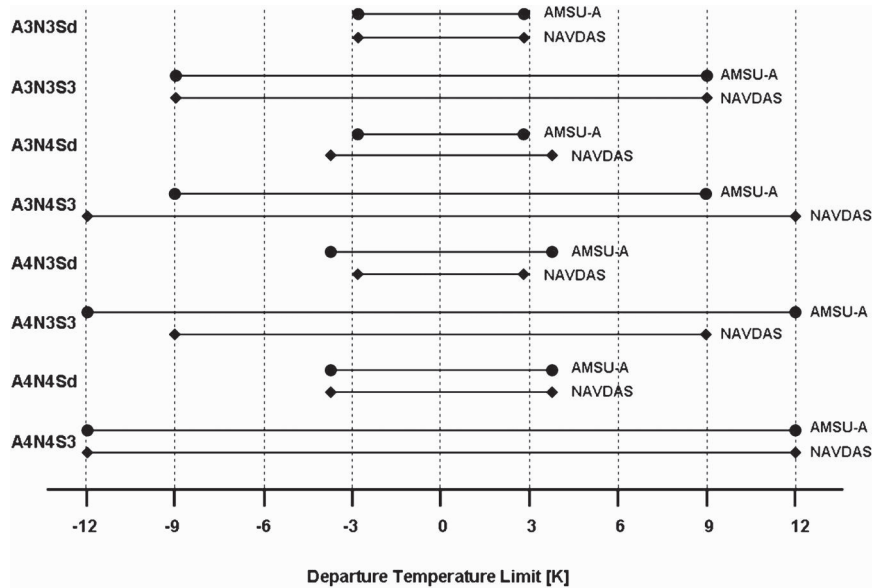


FIG. 7. The ranges of the departure temperature limit (given in Table 2), set by the observation error (σ) and tolerance factors, for each experiment and QC algorithm (AMSU-A or NAVDAS). The “d” in “Sd” represents the default value of 0.95 for σ . See the text for details.

Finally, for the first analysis of each month-long experiment, we used the FNMOC stratospheric analysis above 10 hPa, which is based on the National Environmental Satellite, Data, and Information Service’s (NESDIS) Advanced TIROS (Television Infrared Observation Satellite) Operational Vertical Sounder (ATOVS) temperature retrievals; these retrievals were not used after the initial analysis, and thus the stratosphere may not be represented adequately in the analysis. Normally, the stratospheric jet should have a vertical tilt with height toward the equator, as seen in climatological wind averages (see, e.g., Kim 2007). Because we used the operational physics extended vertically without adding proper middle-atmospheric physics (unlike Kim 2007), our model background may deviate significantly from reality. This vertical jet tilt is, therefore, not represented in both analyses (Fig. 4a) and forecasts (Fig. 4b), and the “error” or “bias” we define in this study may not properly represent true value. Under these conditions, introducing more radiance data of good quality for the bias correction may not efficiently improve the bias in the stratosphere. Gravity-wave drag can alleviate this bias if properly parameterized or calibrated, and can help properly simulate the vertical jet tilt (Kim 2007). We plan to repeat the experiments with improved middle-atmospheric physics to validate this argument.

Acknowledgments. The authors acknowledge the support from the sponsor, the Office of Naval Research,

under ONR Program Elements 0602435N and 0601153N. They appreciate the discussions with and comments from Drs. T. Hogan and N. Baker. They also appreciate the comments from the anonymous reviewers and the evaluation by Dr. D.-L. Zhang. The computing time was provided by the Naval Research Laboratory, Monterey, and the Fleet Numerical Meteorology and Oceanography Center.

APPENDIX A

The Bias Correction/Quality Control Procedures for AMSU-A Radiance Data in NOGAPS/NAVDAS

We list here the procedures related to the AMSU-A bias correction and quality control processes. Note that these procedures are serial—applied to one observation at a time—so that the entire distribution of the innovations of the day is *not* known at the time of the innovation check. The innovation check is therefore not relative to the mean bias-corrected innovation of the day, but relative to zero. More details can be found in Baker and Campbell (2004) or Baker et al. (2005).

- 1) Data are read in and downsampled by a factor of 4 or 5 by skipping beam positions (Fig. 2a).
- 2) Data are further downsampled to a user-controlled density of about one radiance observation per channel

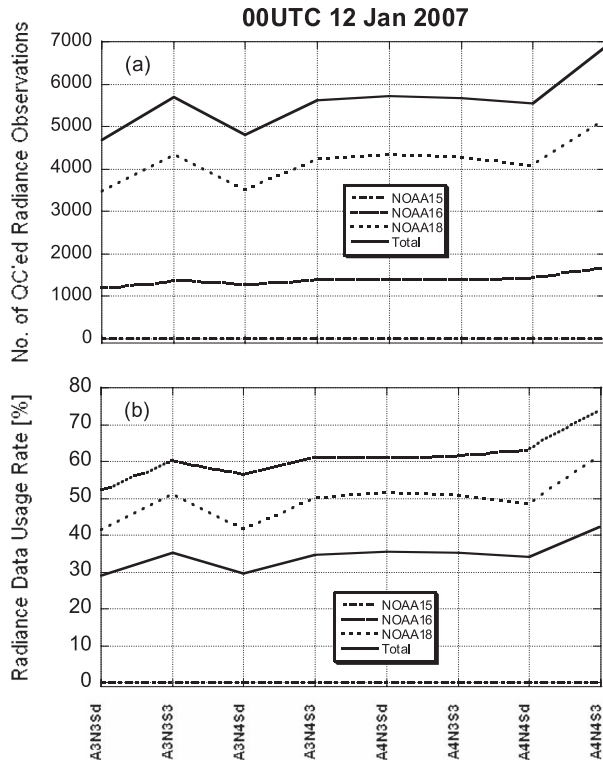


FIG. 8. Graph of (a) the total number of satellite radiance observations for the AMSU-A channel 14 at 0000 (± 3 h) UTC 12 Jan 2007 and (b) the corresponding usage rates for each experiment.

per 165 km \times 165 km area ($1.5^\circ \times 1.5^\circ$ at the equator) per hour (Fig. 2b).

- 3) QC checks related to bad beam position, bad zenith angle, high terrain (higher than 850 hPa), and bad surface skin temperature are applied.
- 4) Scan correction is applied (a single offset at each beam position), which is obtained from the training

- run for the bias coefficients. It is a 15-day global average at each beam position minus the 15-day global average of the two center beam positions.
- 5) The radiative transfer (RT) model [version 6 of the Radiative Transfer Model for TOVS (RTTOV-6)] is called at all of the unflagged observation locations, and if it fails, a QC flag is set. The RT model gives the background brightness temperatures, a subset of which appears in Fig. 2f.
- 6) Land and sea ice QC is applied using the model fields. Selected channels are rejected based on the fields of view, which can consist of land, ocean, sea ice, or land-snow.
- 7) The model-based bias predictors (850–300- and 200–50-hPa thicknesses) are computed at each unflagged observation location, and are multiplied by the so-called air mass coefficients, which were calculated from the previous 15 days of innovations, and then summed with the scan-corrected brightness temperatures to form the bias-corrected brightness temperatures, a subset of which appears in Fig. 2e.
- 8) Gross temperature and gross innovation checks, emissivity, cloud liquid water content, and scattering checks are performed, followed by the innovation check (a.k.a. a rogue or outlier check).
- 9) Any observation location that got flagged in (3)–(8) is plotted in Fig. 2c.
- 10) Any unflagged observations are plotted in Fig. 2d.
- 11) Unflagged observed brightness temperatures from (7) are plotted in Fig. 2e.
- 12) Unflagged background brightness temperatures from (5) are plotted in Fig. 2f.
- 13) The background brightness temperatures are subtracted from the observed brightness temperatures to form the scan-corrected innovation (Fig. 2g).

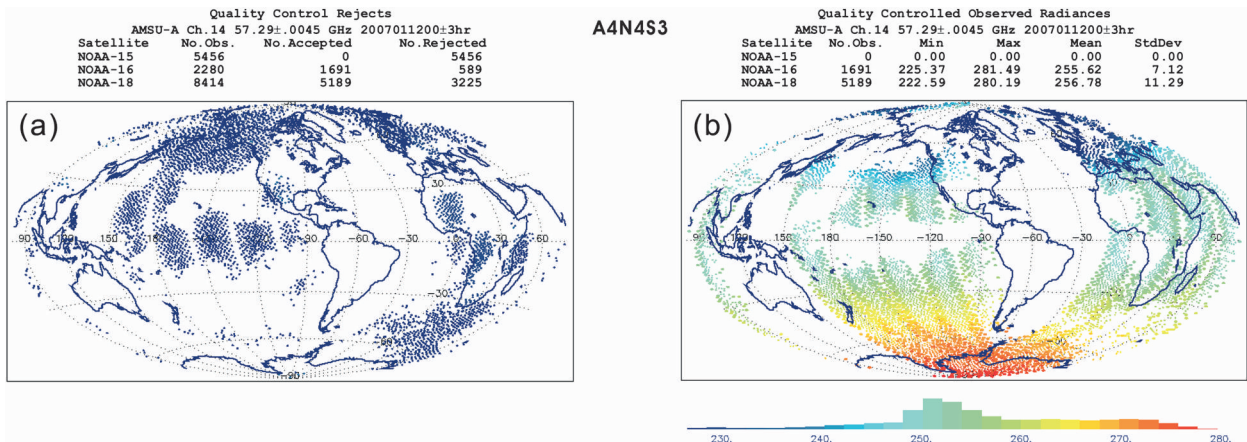


FIG. 9. (a),(b) As in Figs. 2c and 2d, but for A4N4S3.

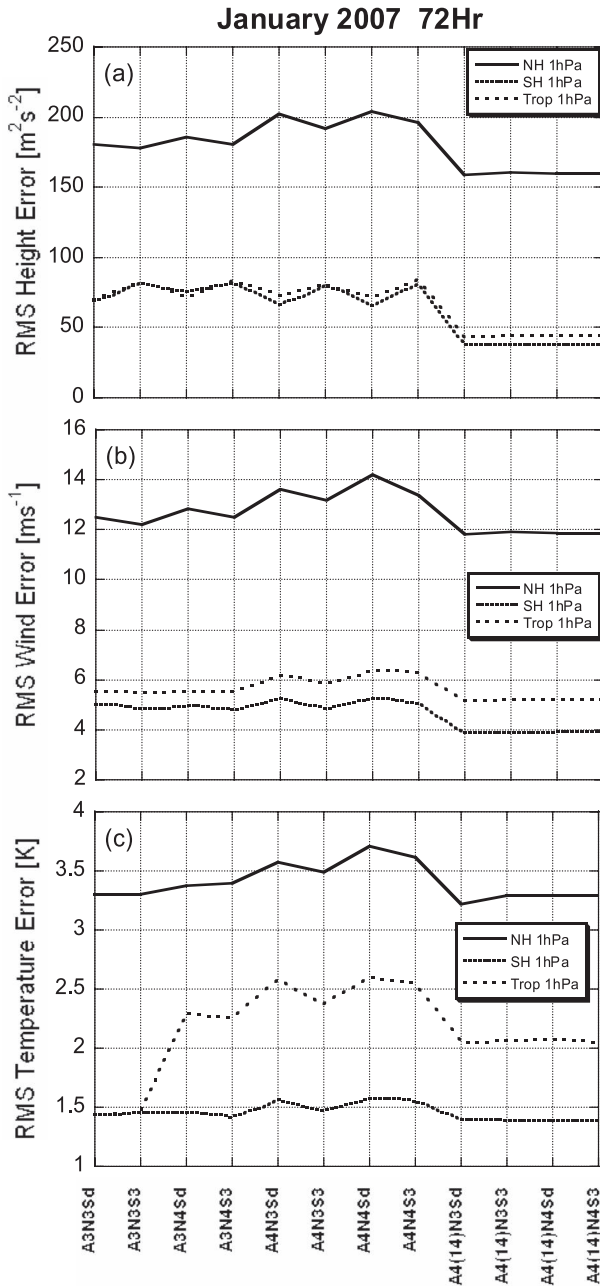


FIG. 10. RMS errors of the 72-h forecasts for January 2007 for the (a) geopotential height ($m^2 s^{-2}$), (b) vector wind ($m s^{-1}$), and (c) temperature (K) at 1 hPa in the Northern Hemisphere (NH; $20^\circ \sim 80^\circ N$), Southern Hemisphere (SH; $20^\circ \sim 80^\circ S$), and tropics (Trop; $20^\circ S \sim 20^\circ N$).

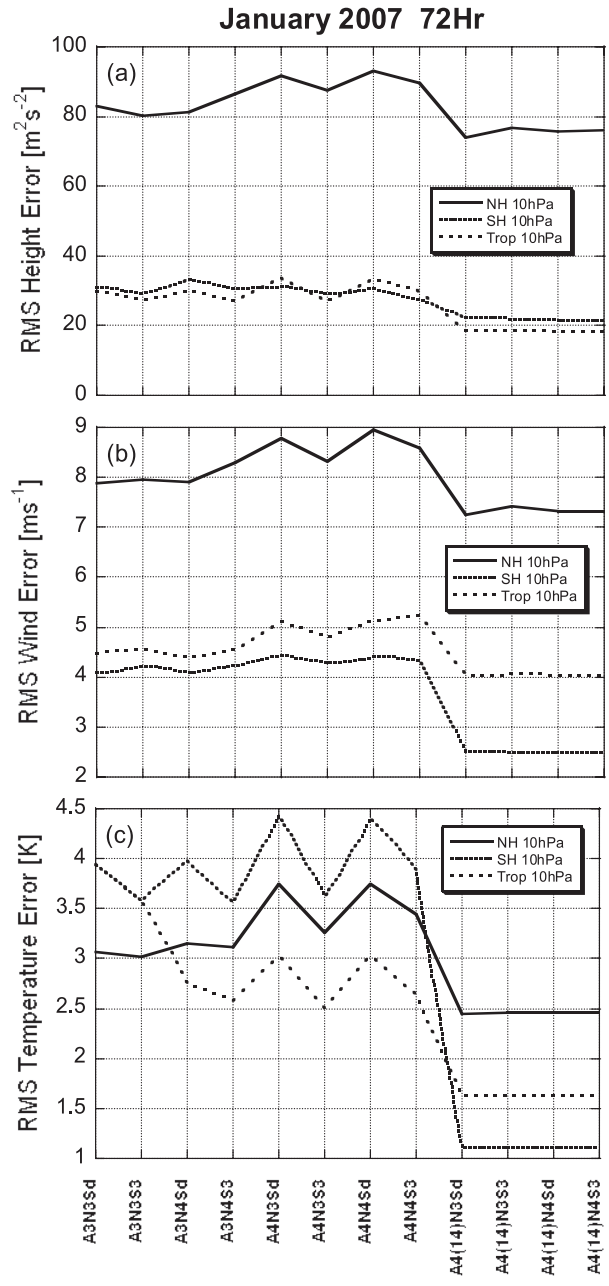


FIG. 11. As in Fig. 10, but at 10 hPa.

14) The background brightness temperatures are subtracted from the bias-corrected observed brightness temperatures to form the final innovation (Fig. 2h) that is presented to the three-dimensional variational data assimilation (3DVAR) scheme, along with the rest of the innovation vector formed by other observation types.

APPENDIX B

A Description of the Analysis Equations for NOGAPS/NAVDAS

a. Basic theories of three-dimensional variational data assimilation

Given N observations of a scalar variable x with known observation error $\epsilon_n = x_n - x$, which is random, unbiased

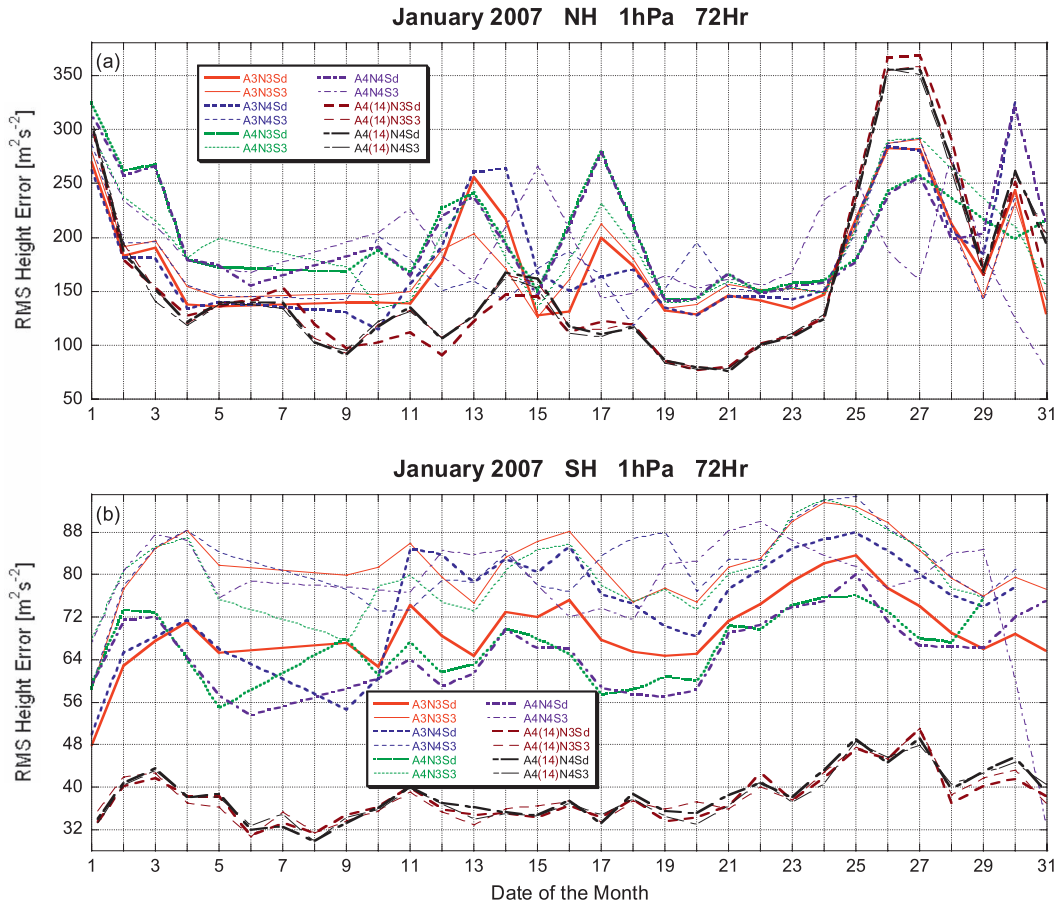


FIG. 12. Time series of the RMS height errors at 1 hPa from the 72-h forecasts for January 2007 for the (a) NH and (b) SH.

($\langle \varepsilon_n \rangle = 0$), and normally distributed, the probability of an error ε_n can be expressed by

$$p(\varepsilon_n) = \frac{1}{\sqrt{2\pi}\sigma_n} \exp\left(\frac{-\varepsilon_n^2}{2\sigma_n^2}\right); \quad \sigma_n^2 = \langle (x_n - x)^2 \rangle = \langle \varepsilon_n^2 \rangle. \quad (B1)$$

If $N = 1$, the most probable value of x is the x that was observed (i.e., $x = x_1$). For $N > 1$, the joint probability that ε_1 lies between ε'_1 and $\varepsilon'_1 + d\varepsilon'_1$, ε_2 lies between ε'_2 and $\varepsilon'_2 + d\varepsilon'_2$, ..., and ε_N lies between ε'_N and $\varepsilon'_N + d\varepsilon'_N$ is simply the product of the individual probabilities, p , assuming that the ε_n are independent. We will mainly be concerned with the case $N = 2$, so that

$$p(\varepsilon_1, \varepsilon_2) = p(\varepsilon_1) \times p(\varepsilon_2) = \frac{1}{2\pi\sigma_1\sigma_2} \exp\left\{-\left[\frac{1}{2}\left(\frac{\varepsilon_1^2}{\sigma_1^2} + \frac{\varepsilon_2^2}{\sigma_2^2}\right)\right]\right\}. \quad (B2)$$

The probability is a maximum when the term inside the braces is a minimum. We can pull out that term,

using the definition of $\varepsilon_n = x_n - x$ to write a quadratic cost function, which we will subsequently minimize to find the most likely x given x_1 and x_2 . We rewrite x_1 and x_2 as x_b to define and minimize the scalar cost function J as

$$J(x) = \frac{1}{2} \left[\frac{(x_b - x)^2}{\sigma_b^2} + \frac{(y - x)^2}{\sigma_y^2} \right], \quad \frac{dJ}{dx} \Big|_{x=x_a} = - \left(\frac{x_b - x}{\sigma_b^2} + \frac{y - x}{\sigma_y^2} \right) \Big|_{x=x_a} = 0. \quad (B3)$$

Solving for x_a and rearranging terms yields

$$x_a = x_b + \frac{\sigma_b^2}{\sigma_b^2 + \sigma_y^2} (y - x_b). \quad (B4)$$

The analysis (x_a) is equal to the background or prior (x_b) plus the weighted innovation ($y - x_b$). If the background value is perfect, $\sigma_b = 0$ and $x_a = x_b$. If the observation is perfect, $\sigma_y = 0$ and $x_a = x_b + 1(y - x_b) = y$.

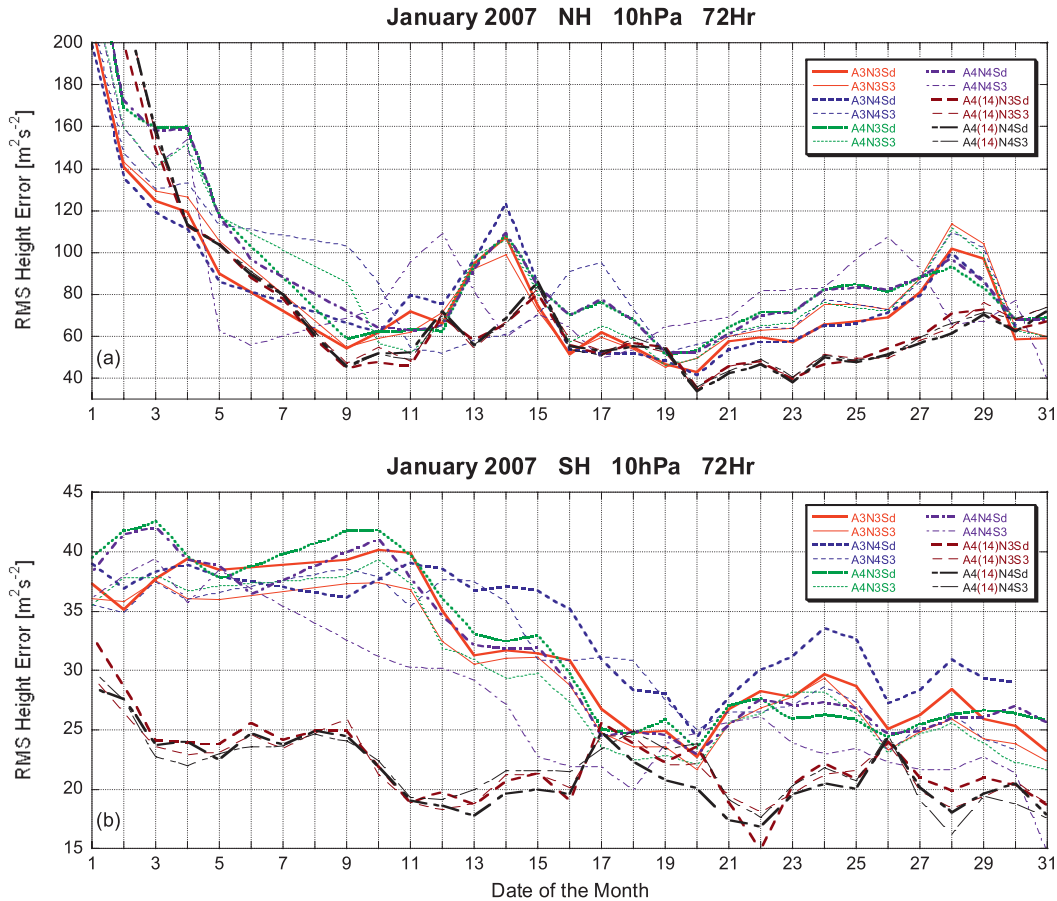


FIG. 13. As in Fig. 12, but for 10 hPa.

If the background and observations are equally uncertain, $\sigma_b = \sigma_y$ and $x_a = \frac{1}{2}(x_b + y)$. We rewrite J in anticipation of going from a scalar x to a vector \mathbf{x} :

$$J(\mathbf{x}) = \frac{1}{2}[(y - x)R^{-1}(y - x) + (x_b - x)P_b^{-1}(x_b - x)], \tag{B5}$$

where $R = \sigma_y^2$, $P_b = \sigma_b^2$. Here, R is the variance of the scalar observation y , and P_b is the variance of the scalar background estimate x_b . Then, the solution can be expressed as

$$x_a = x_b + P_b(P_b + R)^{-1}(y - x_b). \tag{B6}$$

Now let the vector \mathbf{x} be of length K . For each component of \mathbf{x} , there is one background value x_b and (assume for now) one observation y_k ($N = 2$), so that there are two sources of information for each of the many different variables listed in \mathbf{x} . We let \mathbf{P}_b be the background error covariance matrix, which relates forecast errors for a given variable and location to other forecast variables and locations:

$$\mathbf{P}_b = \begin{pmatrix} \sigma_{b_1}^2 & c_{b_1 b_2} & \cdots & c_{b_1 b_K} \\ c_{b_2 b_1} & \sigma_{b_2}^2 & & \vdots \\ \vdots & & \ddots & \vdots \\ c_{b_K b_1} & \cdots & \cdots & \sigma_{b_K}^2 \end{pmatrix}. \tag{B7}$$

Note that although this matrix is reasonably sparse, it has many nonzero off-diagonal elements, making it non-trivial to invert. Similarly, we let \mathbf{R} be the observation error covariance matrix, which is typically taken to be diagonal. We write down the probability distributions, assuming $\boldsymbol{\varepsilon}_b$ and $\boldsymbol{\varepsilon}_y$ are independent (a good assumption):

$$p(\boldsymbol{\varepsilon}_b, \boldsymbol{\varepsilon}_y) = p(\boldsymbol{\varepsilon}_b) \times p(\boldsymbol{\varepsilon}_y) \propto \exp\left\{-\left[\frac{1}{2}(\boldsymbol{\varepsilon}_b^T \mathbf{R}^{-1} \boldsymbol{\varepsilon}_b + \boldsymbol{\varepsilon}_y^T \mathbf{P}_b^{-1} \boldsymbol{\varepsilon}_y)\right]\right\}. \tag{B8}$$

As before, we define a quadratic cost function, whose minimization will find the most probable (maximum likelihood) analysis:

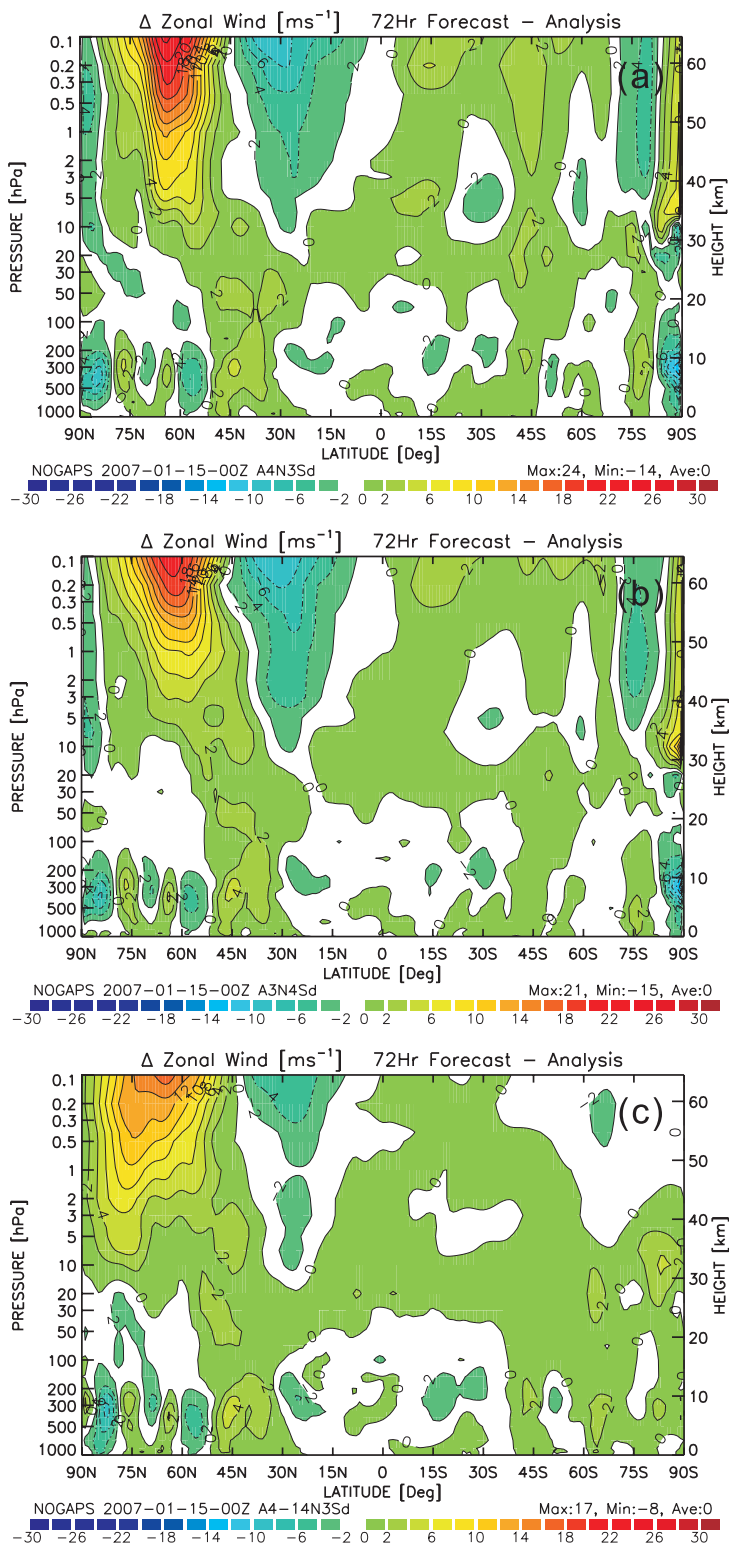


FIG. 14. The 72-h forecast minus analysis result of the zonal-mean zonal wind for (a) A4N3Sd, (b) A3N4Sd, and (c) A4(14)N3Sd (cf. with Fig. 4c).

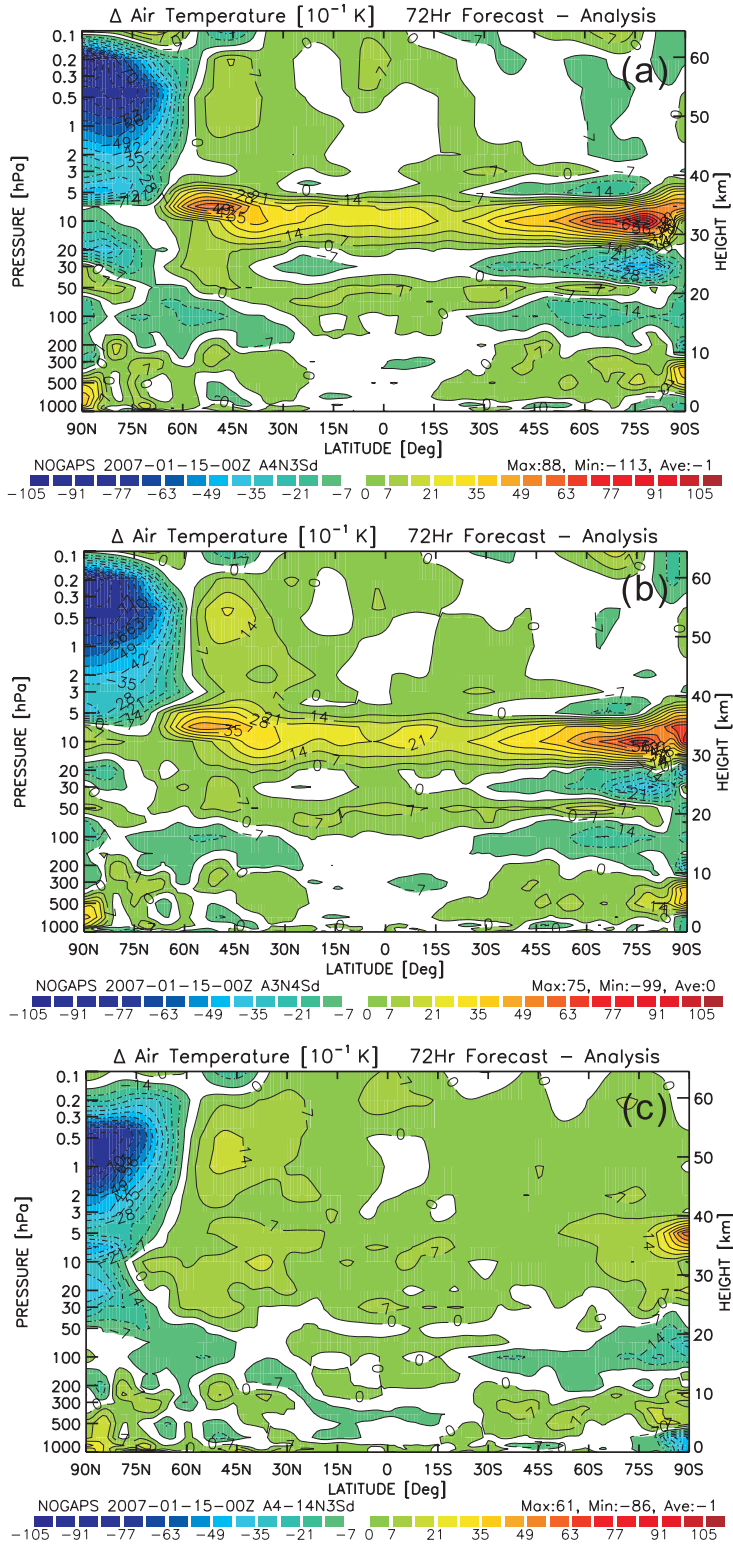


FIG. 15. As in Fig. 14, but for the temperature (cf. with Fig. 5c).

TABLE 3. The biases in the zonal-mean zonal wind and temperature fields in terms of the difference between the maximum and minimum field values of the model bias (i.e., forecast – analysis). The cases A3N4Sd, A4N3Sd, and A4(14)N3Sd correspond to Figs. 14 and 15.

Expt	$(U_F - U_A)_{\max}$	$(U_F - U_A)_{\min}$	$\frac{(U_F - U_A)_{\max} - (U_F - U_A)_{\min}}{(U_F - U_A)_{\min}}$	$(T_F - T_A)_{\max}$	$(T_F - T_A)_{\min}$	$\frac{(T_F - T_A)_{\max} - (T_F - T_A)_{\min}}{(T_F - T_A)_{\min}}$
A3N3Sd	29	-14	43	7.4	-8.7	16.1
A3N3S3	22	-15	37	7.8	-8.2	16.0
A3N4Sd	21	-15	36	7.5	-9.9	17.4
A3N4S3	19	-14	33	7.7	-6.9	14.6
A4N3Sd	24	-14	38	8.8	-11.3	20.1
A4N3S3	22	-13	35	7.0	-10.0	17.0
A4N4Sd	24	-15	39	11.4	-11.4	22.8
A4N4S3	23	-10	33	9.3	-10.5	19.8
A4(14)N3Sd	17	-8	25	6.1	-8.6	14.7
A4(14)N3S3	18	-8	26	6.6	-8.9	15.5
A4(14)N4Sd	18	-9	27	6.5	-8.8	15.3
A4(14)N4S3	17	-9	26	6.7	-8.9	15.6

$$J(\mathbf{x}) = \frac{1}{2}[(\mathbf{y} - \mathbf{x})^T \mathbf{R}^{-1}(\mathbf{y} - \mathbf{x}) + (\mathbf{x}_b - \mathbf{x})^T \mathbf{P}_b^{-1}(\mathbf{x}_b - \mathbf{x})]. \tag{B9}$$

We set the partial derivative of J with respect to each component equal to zero, and solve for \mathbf{x}_a :

$$\mathbf{x}_a = (\mathbf{P}_b^{-1} + \mathbf{R}^{-1})^{-1}(\mathbf{P}_b^{-1}\mathbf{x}_b + \mathbf{R}^{-1}\mathbf{y}). \tag{B10}$$

Rewriting using the Sherman–Morrison–Woodbury identity yields

$$\mathbf{x}_a = \mathbf{x}_b + \mathbf{P}_b(\mathbf{P}_b + \mathbf{R})^{-1}(\mathbf{y} - \mathbf{x}_b). \tag{B11}$$

For some conventional observations like a temperature measurement from a weather balloon, \mathbf{y} and \mathbf{x}_b are the same variable, although the background values typically will have to be interpolated to the observation locations. For other observations, such as the microwave radiances discussed in this study, a more complex forward operator \mathcal{H} is needed to convert between observational and model variables. Here, \mathcal{H} can include horizontal, vertical, and temporal interpolation; radiative transfer; integration; or any function relating an observed variable to model quantities. Thus, in (B11), we need to include the full-forward operator and its Jacobian \mathbf{H} (the partial derivatives of \mathcal{H} with respect to all of its inputs) as follows:

$$\mathbf{x}_a = \mathbf{x}_b + \mathbf{P}_b \mathbf{H}^T (\mathbf{H} \mathbf{P}_b \mathbf{H}^T + \mathbf{R})^{-1} [\mathbf{y} - \mathcal{H}(\mathbf{x}_b)]. \tag{B12}$$

b. Application to NAVDAS

Here, we relax the earlier assumption that we have one observation for each model variable and location, so \mathbf{H} will be a rectangular matrix with dimensions $K \times M$,

where K is the number of observations (typically ~300 000 for operational NAVDAS in 2007) and M is the dimension of the model state vector (typically 30 000 000 for operational NOGAPS in 2007). Equation (B12) is the equation for three-dimensional variational data assimilation solved by NAVDAS (Daley and Barker 2001a,b). Essentially, it consists of a weighted, covarying least squares fit between the forecast and the observed data. Because of its size, we do not explicitly form the full \mathbf{P}_b matrix, although we can calculate any given element we need. The solution of (B12) can be broken down into three steps.

First, we compute the *innovation vector* $[\mathbf{y} - \mathcal{H}(\mathbf{x}_b)]$. For microwave radiances, this includes interpolation and solving the radiative transfer equations to obtain the forecast values in radiance space. The observed radiances must be bias corrected; we use a method based on Harris and Kelly (2001). Linear regression of 15 days of raw innovation data using 850–300- and 200–50-hPa thicknesses as predictors yields a constant plus two coefficients for each channel of the AMSU-A instrument. For scan bias, the difference between the 15-day mean at beam positions x and the two center beam positions is subtracted from beam position x for each instrument. We apply this simple scan bias correction to the current observations in each channel and, then, apply the linear regression coefficients as follows to form the bias-corrected innovations:

$$[\mathbf{y}_s - (c_o + c_1 p_1 + c_2 p_2)] - \mathcal{H}(\mathbf{x}_b), \tag{B13}$$

where \mathbf{y}_s is the scan-corrected observation and $c_o + c_1 p_1 + c_2 p_2$ are the linear regression coefficients times the predictors, forming the bias-corrected observation. Next, we solve the following linear system for \mathbf{z} using an iterative method (preconditioned conjugate gradient descent):

$$[\mathbf{H}\mathbf{P}_b\mathbf{H}^T + \mathbf{R}]\mathbf{z} = \mathbf{y} - \mathcal{H}(\mathbf{x}_b). \quad (\text{B14})$$

Note that the right-hand side of (B14) is (B13), the bias-corrected innovation vector. This step is the most time-consuming and memory-intensive part of NAVDAS. Finally, we perform a postmultiplication step to obtain the correction, which is added to the background \mathbf{x}_b to form the analysis \mathbf{x}_a :

$$\mathbf{x}_a = \mathbf{x}_b + \mathbf{P}_b\mathbf{H}^T\mathbf{z}. \quad (\text{B15})$$

Like any least squares method, the analysis is sensitive to outliers, implying that the proper quality control and bias correction of data are essential. Quality control can include gross error checks, buddy checks, self-consistency checks, and statistically based checks (rogue checks). Appendix A describes the details of these checks. The reader is referred to the main text for application and discussion of these concepts.

REFERENCES

- Auligné, T., and A. P. McNally, 2007: Interaction between bias correction and quality control. *Quart. J. Roy. Meteor. Soc.*, **133**, 643–653.
- Baker, N. L., and W. F. Campbell, 2004: The impact of AMSU-A radiance assimilation in the U.S. Navy's Operational Global Atmospheric Prediction System (NOGAPS). Preprints, *13th Conf. on Satellite Meteorology and Oceanography*, Norfolk, VA, Amer. Meteor. Soc., P3.1. [Available online at <http://ams.confex.com/ams/pdfpapers/80714.pdf>.]
- , T. F. Hogan, W. F. Campbell, R. L. Pauley, and S. D. Swadley, 2005: The impact of AMSU-A radiance assimilation in the U.S. Navy's Operational Global Atmospheric Prediction System (NOGAPS). NRL Memo. Rep. NRL/MR/7530-05-8836, 18 pp. [Available from Naval Research Laboratory, Monterey, CA 93943-5502.]
- Daley, R., and E. Barker, 2001a: NAVDAS Source Book 2001: The NRL Atmospheric Variational Data Assimilation System. NRL Publication NRL/PU/7530-00-418, 160 pp. [Available from Marine Meteorology Division, NRL, Monterey, CA 93943-5502.]
- , and —, 2001b: NAVDAS: Formulation and diagnostics. *Mon. Wea. Rev.*, **129**, 869–883.
- Dee, D. P., 2005: Bias and data assimilation. *Quart. J. Roy. Meteor. Soc.*, **131**, 3323–3343.
- , and S. Uppala, 2008: Variational bias correction in ERA—Interim. ECMWF Tech. Memo. 575, 28 pp.
- Harris, B. A., and G. Kelly, 2001: A satellite bias correction scheme for radiance assimilation. *Quart. J. Roy. Meteor. Soc.*, **127**, 1453–1468.
- Hogan, T. F., and T. E. Rosmond, 1991: The description of the Navy Operational Global Atmospheric Prediction System's spectral forecast model. *Mon. Wea. Rev.*, **119**, 1786–1815.
- Kim, Y.-J., 2007: Balance of drag between the middle and lower atmospheres in a global atmospheric forecast model. *J. Geophys. Res.*, **112**, D13104, doi:10.1029/2007JD008647.
- , and T. F. Hogan, 2004: Response of a global atmospheric forecast model to various drag parameterizations. *Tellus*, **56A**, 472–484.